10-26-2020

Riluzole attenuates glutamatergic tone and cognitive decline in AβPP/PS1 mice.

Kevin N Hascup

Caleigh A Findley

Jesse Britz

Nahayo Esperant-Hilaire

Sarah O Broderick

See next page for additional authors

Recommended Citation

Hascup, Kevin N, Findley, Caleigh A, Britz, Jesse, Esperant-Hilaire, Nahayo, Broderick, Sarah O, Delfino, Kristin, Tischkau, Shelley, Bartke, Andrzej and Hascup, Erin R. "Riluzole attenuates glutamatergic tone and cognitive decline in AβPP/PS1 mice.." *Journal of neurochemistry* (Oct 2020). doi:10.1111/jnc.15224.

Received: 27 April 2020 | Revised: 17 September 2020 | Accepted: 9 October 2020

DOI: 10.1111/jnc.15224

ORIGINAL ARTICLE

Journal of Neurochemistry JNC The Official Journal of the International Society for Neurochemistry WILEY

Riluzole attenuates glutamatergic tone and cognitive decline in AβPP/PS1 mice

Kevin N. Hascup[1,2,3] | Caleigh A. Findley[1,2] | Jesse Britz[2] | Nahayo Esperant-Hilaire[1] | Sarah O. Broderick[1] | Kristin Delfino[4] | Shelley Tischkau[2,3] | Andrzej Bartke[3,5] | Erin R. Hascup[1,2]

[1]Department of Neurology, Center for Alzheimer's Disease and Related Disorders, Neurosciences Institute, Southern Illinois University School of Medicine, Springfield, IL, USA

[2]Department of Pharmacology, Southern Illinois University School of Medicine, Springfield, IL, USA

[3]Department of Medical Microbiology, Immunology and Cell Biology, Southern Illinois University School of Medicine, Springfield, IL, USA

[4]Department of Surgery, Center for Clinical Research, Southern Illinois University School of Medicine, Springfield, IL, USA

[5]Department of Internal Medicine, Southern Illinois University School of Medicine, Springfield, IL, USA

Correspondence
Erin R. Hascup, Department of Neurology, Center for Alzheimer's Disease and Related Disorders, Southern Illinois University School of Medicine, P.O. Box 19628, Springfield, IL 62794-9628, USA.
Email: ehascup@siumed.edu

Funding information
Kenneth Stark Endowment; William E. McElroy Foundation; SIU Foundation at the School of Medicine; Center for Alzheimer's Disease and Related Disorders; National Institute on Aging, Grant/Award Number: R01AG057767 and R01AG061937

Abstract

We have previously demonstrated hippocampal hyperglutamatergic signaling occurs prior to plaque accumulation in AβPP/PS1 mice. Here, we evaluate 2-Amino-6-(trifluoromethoxy) benzothiazole (riluzole) as an early intervention strategy for Alzheimer's disease (AD), aimed at restoring glutamate neurotransmission prior to substantial Beta amyloid (Aβ) plaque accumulation and cognitive decline. Male AβPP/PS1 mice, a model of progressive cerebral amyloidosis, were treated with riluzole from 2–6 months of age. Morris water maze, in vivo electrochemistry, and immunofluorescence were performed to assess cognition, glutamatergic neurotransmission, and pathology, respectively, at 12 months. Four months of prodromal riluzole treatment in AβPP/PS1 mice resulted in long-lasting procognitive effects and attenuated glutamatergic tone that was observed six months after discontinuing riluzole treatment. Riluzole-treated AβPP/PS1 mice had significant improvement in long-term memory compared to vehicle-treated AβPP/PS1 mice that was similar to normal aging C57BL/6J control mice. Furthermore, basal glutamate concentration and evoked-glutamate release levels, which were elevated in vehicle-treated AβPP/PS1 mice, were restored to levels observed in age-matched C57BL/6J mice in AβPP/PS1 mice receiving prodromal riluzole treatment. Aβ plaque accumulation was not altered with riluzole treatment. This study supports that interventions targeting the glutamatergic system during the early stages of AD progression have long-term effects on disease outcome, and importantly may prevent cognitive decline. Our observations provide preclinical support for targeting glutamate neurotransmission in patients at risk for developing AD.

KEYWORDS

alpha-7 nicotinic acetylcholine receptor (α7nAChR), Alzheimer's disease (AD), amyloid-beta (Aβ), biosensor, learning and memory, prodromal intervention

Abbreviations: AA, L-ascorbic acid; AD, Alzheimer's disease; ALS, amyotrophic lateral sclerosis; Aβ, beta amyloid; BSA, bovine serum albumin; CIPL, corrected integrated path length; DA, dopamine hydrochloride; FAST, Fast Analytical Sensing Technology; GFAP, glial fibrillary acidic protein; GLT-1, glutamate transporter-1; Glu/Gln, glutamate/glutamine; H_2O_2, hydrogen peroxide; KCl, potassium chloride; MWM, Morris water maze; NMDA, *N*-methyl-D-aspartate; PBS, phosphate-buffered saline; α7nAChR, alpha 7 nicotinic receptor.

Kevin N. Hascup and Caleigh A. Findley contributed equally to the manuscript.

1 | INTRODUCTION

Alzheimer's disease (AD) is an age-related neurodegenerative disorder resulting in a gradual buildup of Aβ plaques and neurofibrillary tangles followed by hippocampal atrophy and progressive dementia (Jack et al., 2013; Mota et al., 2014). Current pharmacotherapy options include cholinesterase inhibitors aimed at increasing acetylcholine levels and preventing glutamate-induced excitotoxicity through *N*-methyl-D-aspartate (NMDA) receptor antagonism (Godyń et al., 2016). However, these therapies have limited efficacy, are symptomatic, and do not decelerate disease progression, which may be a consequence of administration at advanced AD stages when synapse loss is extensive. To slow or stop AD progression, it may be necessary to target neurological components that are altered during the prodromal phase of AD. Increasing evidence supports the glutamatergic system as a possible early target that meets these criteria (Hascup et al., 2019, 2020; Minkeviciene et al., 2008; Paula-Lima et al., 2013).

Alterations to glutamate release and clearance may lead to the cognitive and functional decline observed in AD (Hascup et al., 2019, 2020; Hunsberger et al., 2015; Miller et al., 2008; O'Brien et al., 2010). A prevailing hypothesis in AD research supports persistent, excessive activation of NMDA receptors impedes the detection of physiological signals and initiating cognitive impairment (Olney et al., 1997; Parameshwaran et al., 2008; Parsons et al., 2007; Talantova et al., 2013; Winblad & Poritis, 1999). Several studies have observed hippocampal hyperactivity in mild cognitively impaired patients (Huijbers et al., 2015; Miller et al., 2008; O'Brien et al., 2010), particularly those with a familial history of AD (Okonkwo et al., 2014) and elevated amyloid-beta (Aβ) deposition (Huijbers et al., 2015), that is associated with increased severity of cognitive decline (Huijbers et al., 2015; Miller et al., 2008; O'Brien et al., 2010). Previous data support that accumulation of soluble Aβ isoforms underlie synaptic dysfunction and eventual neurodegeneration (Yang et al., 2017). Our laboratory and others have demonstrated that soluble $A\beta_{42}$ elicits glutamate release through the alpha-7 nicotinic acetylcholine receptor (α7nAChR) (Hascup & Hascup, 2016; Mura et al., 2012; Talantova et al., 2013), which may contribute to elevated levels of hippocampal glutamate first observed prior to cognitive decline in double transgenic mice expressing the amyloid precursor protein (Mo/HuAPP695swe) and Presenilin 1 (PS1-dE9) genes (AβPP/PS1). Furthermore, we have also reported subregion and age specific alterations in hippocampal glutamatergic activity in AβPP/PS1. Elevated dentate (DG) and CA1 evoked glutamate release is observed at 2–4 months of age, while elevated basal glutamate in observed in these regions by 6 months of age (Hascup et al., 2020). These elevated levels continue to 12 months of age (Hascup et al., 2018, 2019), when cognitive deficits are more pronounced. These findings indicate early alterations to the glutamatergic system evolve throughout disease progression as in AβPP/PS1 mice. Furthermore, it supports the hypothesis that elevation of synaptic glutamate levels over time may result in excitotoxicity and eventual hippocampal atrophy observed in AD.

Attenuating glutamatergic tone by targeting glutamate release and uptake may provide promising therapeutic interventions for early AD. One possible intervention is 2-Amino-6-(trifluoromethoxy) benzothiazole (riluzole), which is thought to inhibit presynaptic excitation (Bellingham & Walmsley, 1999; Ireland et al., 2004) and glutamate release (Bellingham, 2011; Wang et al., 2004), while also restoring transporter expression and activity (Carbone et al., 2012a; Fumagalli et al., 2008; Frizzo et al., 2004). Furthermore, riluzole has previously shown to attenuate $A\beta_{42}$-mediated increases in CA1 spike frequency and restore the DG excitatory/ inhibitory imbalance resulting in improved cognitive performance (Ren et al., 2015; Yang et al., 2020). Based on these previous studies, we hypothesized that riluzole treatment has long-term procognitive benefits mediated by reducing the glutamatergic tone in amyloidogenic AD mice.

In this study, AβPP/PS1 mice were treated with riluzole (2–6 months of age) prior to the onset of cognitive deficits (Minkeviciene et al., 2008; Webster et al., 2014). Starting at 12 months of age, mice underwent Morris water maze (MWM) spatial learning and memory paradigm to assess cognition. This experimental design emphasizes a preventative approach to ameliorating the glutamatergic dyshomeostasis and cognitive decline observed at 12 months of age in this mouse model (Hascup et al., 2018, 2019; Minkeviciene et al., 2008; Webster et al., 2014). In vivo hippocampal glutamate signaling was assessed using constant potential amperometry followed by immunofluorescence to examine hippocampal Aβ plaque burden and expression of several glutamatergic synaptic factors. The results presented here support that prodromal riluzole treatment has long-term procognitive efficacy by reducing hippocampal glutamatergic tone.

2 | METHODS

2.1 | Animals

Male C57BL/6J (RRID:IMSR_JAX:000664) and AβPP/PS1 (RRID:MMRRC_034832-JAX) mice were obtained from Jackson Laboratory. Protocols for animal use were approved by the *Laboratory Animal Care and Use Committee* at Southern Illinois University School of Medicine (Protocol #219-13-012) and the study was not pre-registered. Mice were group-housed on a 12:12 hr light: dark cycle, and food and water were available ad libitum. All experiments were conducted during the light phase. A timeline of the experimental design is presented in Figure 1. From 2 to 6 months of age, a randomly assigned cohort of AβPP/PS1 mice was given riluzole in the drinking water (12.5 mg/kg b.w./day in 1% sucrose; $n = 11$). C57BL/6J ($n = 14$) and the other cohort of AβPP/PS1 ($n = 12$) mice were given 1% sucrose in the drinking water as vehicle control. Three mouse cages were pseudo-randomized using the Microsoft Excel randomization function to generate random decimal numbers between 0 and 1 for each cage and treatment. The dosing strategy was based on previously published studies using riluzole in vivo (Gourley et al., 2011; Hunsberger

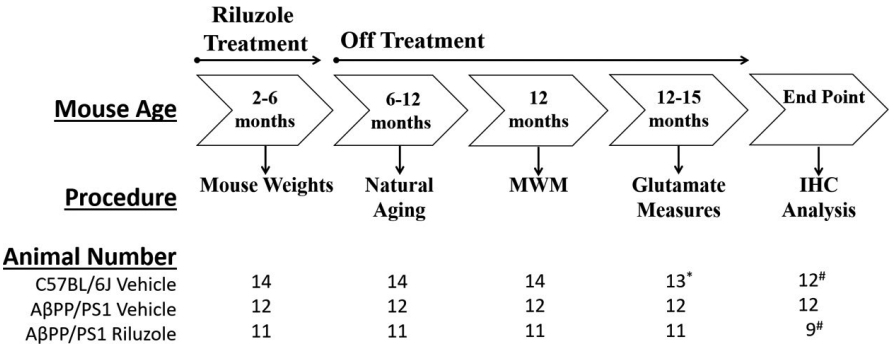

FIGURE 1 Experimental design. An outline of the experimental design. Riluzole treatment was conducted when mice were 2–6 months of age. At 6 months of age, treatment was discontinued and mice were returned to untreated water for the remainder of the study. Animal numbers are located underneath each analysis. *One C57BL/6J vehicle treated mouse died due to complications from anesthetized surgical procedures. #One C57BL/6J vehicle treated and two AβPP/PS1 mice were excluded from immunofluorescent analysis because of inadequate slice preparation and staining procedures. Abbreviations: Morris water maze (MWM)

et al., 2015; Ishiyama et al., 2004). No exclusion criteria were predetermined. All mice underwent cognitive assessment, in vivo glutamate recordings, and immunofluorescent analysis except for one C57BL/6J vehicle mouse was not used for glutamate measures because it died due to surgical complications and 3 mice (1 C57BL/6J vehicle and 2 AβPP/PS1 riluzole) were excluded from immunofluorescence because of inadequate sectioning or staining. Immediately following anesthetized glutamate recordings, mice were euthanized with an overdose of isoflurane followed by rapid decapitation. A 5 mm tail snip was sent to TransnetYX®, Inc to confirm genotypes. All mice were tattooed with unique numerical identifiers to blind researchers throughout experimental paradigms.

2.2 | Chemicals

All chemicals were prepared and stored according to manufacturer's recommendations unless otherwise noted. L-glutamate oxidase (EC 1.4.3.11) was obtained from Cosmo Bio Co. (Cat: YMS-80049) and diluted in distilled, deionized water to make a 1 U/μl stock solution for storage at 4°C. Sodium phosphate monobasic monohydrate (Cat: BP330-500), sodium phosphate dibasic anhydrous (Cat: S375-500), 1,3 phenylenediamine dihydrochloride (mPD; Cat: P017225G), sodium chloride (Cat: S271-3), calcium chloride dehydrate (Cat: BP510-100), sucrose (Cat: 12-550-15), 30% hydrogen peroxide (H_2O_2) in water (Cat: H325-100), and riluzole (Cat: 1744-22-5) were obtained from Thermo Fisher Scientific. L-glutamic acid sodium salt (Cat: G1626), potassium chloride (KCl; Cat: P9333), bovine serum albumin (BSA; Cat: A3059), glutaraldehyde (Cat: G5882), dopamine hydrochloride (DA; Cat: H8502), and L-ascorbic acid (AA; Cat: A7056) were obtained from Sigma-Aldrich Co. Chicken polyclonal glial fibrillary acidic protein (GFAP) primary antibody (RRID:AB_2492333) and Amylo-Glo® RTD™ (Cat: TR-300-AG) was obtained from Biosensis. Rabbit polyclonal primary antibody α7nAChR was obtained from Alomone Labs (RRID:AB_10659339).

2.3 | Morris water maze (MWM) training and probe challenge

At approximately 12 months of age, mice underwent cognitive assessment using the MWM spatial learning and memory recall paradigm. The MWM tests spatial learning and memory by requiring the mouse to utilize visual cues to repeatedly swim to a static, submerged platform (Bromley-Brits et al., 2011). The MWM paradigm consisted of 5 consecutive learning days with three, 90-s trials/day and a minimum inter-trial interval of 20 min. After two days without testing, mice are given a single, 60-s probe challenge to test long-term memory recall. The ANY-maze video tracking system (Stoelting Co., RRID:SCR_014289) was used to record navigational parameters and data analysis. The three trials for each training day were averaged for each mouse for analysis. Variables extracted from ANY-maze and utilized for data analysis include swimming speed, platform cumulative distance, platform corrected integrated path length, percent time in quadrant, and annulus 40 entries.

2.4 | Enzyme-based microelectrode arrays

Enzyme-based MEAs were fabricated, assembled, coated, and calibrated for in vivo glutamate measurements as previously described (Hascup & Hascup, 2015, 2016; Hascup et al., 2016, 2018, 2019). One of the R2 MEA Pt sites was coated with L-glutamate oxidase solution [containing BSA and glutaraldehyde for enzyme adhesion] to enzymatically degrade glutamate to α-ketoglutarate and H_2O_2, the electroactive reporter molecule. The second Pt recording site (self-referencing or sentinel site) was coated with a BSA and glutaraldehyde solution, which is unable to enzymatically generate H_2O_2 from L-glutamate. A potential of +0.7 V versus a Ag/AgCl reference electrode was applied to the Pt recording surfaces resulting in oxidation of the H_2O_2 reporter molecule. The subsequent current generated from the two-electron transfer was amplified and digitized by the Fast Analytical Sensing Technology (FAST) 16mkIII (Quanteon; LLC) electrochemistry instrument.

2.5 | mPD electropolymerization

After enzyme coating, all Pt recording surfaces were electroplated with 5 mM mPD in 0.05 M phosphate-buffered saline (PBS). FAST electroplating software applied a triangular wave potential with an offset of −0.5 V, peak-to-peak amplitude of 0.25 V, at a frequency of 0.05 Hz, for 20 min. This created a size exclusion layer that restricts the passage of AA, DA, uric acid, and 3,4-dihydroxyphenylacetic acid to the Pt recording surface (Hascup et al., 2016).

2.6 | Calibration

Each MEA underwent an in vitro calibration prior to implantation to create a standard curve for the conversion of current to glutamate concentration. The Pt recording sites and a glass Ag/AgCl reference electrode (Bioanalytical Systems, Inc.) were placed in a continuously stirred solution of 40.0 ml of 0.05 M PBS maintained at 37°C with a recirculating water bath (Stryker Corp.). Final beaker concentrations of 250 μM AA, 10, 20, 30, and 40 μM L-glutamate, 2 μM DA, and 8.8 μM H_2O_2 were used to assess MEA performance. Thirty-eight MEAs were used with an average ± standard error of the mean (*SEM*) for glutamate sensitivity of 6.0 ± 0.1 pA/μM (r^2 = 0.998 ± 0.001), selectivity ratio of 391 ± 46 to 1, and limit of detection of 0.2 ± 0.02 μM based on a signal-to-noise ratio of 3. A glass micropipette (World Precision Instruments, Inc.) was attached to the MEA and used to locally apply 70 mM KCl (isotonic; pH 7.4) to the mouse hippocampal subfields (Hascup & Hascup, 2015; Hascup et al., 2016, 2018, 2019). The fluid was pressure-ejected using a Picospritzer III (Parker-Hannafin), with pressure (5–15 psi) adjusted to deliver consistent volumes over 1–2 s intervals and monitored with a stereomicroscope (Luxo Corp.) fitted with a calibrated reticule.

2.7 | In vivo anesthetized recordings

Beginning one week after MWM, mice were anesthetized using 1.5%–2.0% isoflurane (Abbott Lab) in a calibrated vaporizer (Vaporizer Sales & Service, Inc., Rockmart, GA) and prepared for in vivo electrochemical recordings (Hascup et al., 2016, 2018, 2019). A Ag/AgCl reference wire was subdurally positioned above the right cortex. For each mouse, the MEA/ micropipette assembly was lowered into the DG (AP: −2.0, ML: ±1.0, DV: −2.2 mm), CA3 (AP: −2.0, ML: ±2.0, DV: −2.2 mm), and CA1 (AP: −2.0, ML: ±1.0, DV: −1.7 mm), from Bregma (Paxinos & Franklin, 2004) that was randomly assigned. Constant voltage amperometry (4 Hz) was performed by using a potential of + 0.7 V versus the Ag/AgCl reference electrode applied by the FAST16mkIII electrochemical instrument (Quanteon LLC). MEAs were allowed to reach a stable baseline for 60 min before a 10-s basal glutamate determination and pressure ejection studies commenced. The FAST software saves amperometric data, time, and pressure ejection events for all recording sites. Calibration data, in conjunction with a MATLAB (MathWorks) graphic user interface program was used to calculate basal glutamate and stimulus-evoked glutamate release and uptake. Five reproducible signals were evoked in each hippocampal subfield and averaged into a representative signal for treatment comparisons.

2.8 | Immunodetection, amyloid plaque staining, and semiquantification

Immediately following in vivo glutamate measurements, brains were fixed in 4% paraformaldehyde for 48 hr and then transferred into 30% sucrose in 0.1M phosphate buffer for 24 hr prior to sectioning (Hascup et al., 2016, 2018, 2019). Primary antibodies were applied to every sixth section (20 μm thickness) from the hippocampus at the following concentrations: chicken polyclonal GFAP antibody (Biosensis; 1:100) or rabbit polyclonal α7nAChR antibody (Alomone Labs; 1:200). Slides were treated with 10% H_2O_2 in 20% methanol for 10 min and then transferred to a 70% ethanol solution for 5 min followed by a 2 min wash in PBS. Sections were incubated for 10 min in 1× Amylo-Glo® RTD™ and rinsed in 0.9% saline for 5 min without shaking followed by rinsing (3 × 2 min) in PBS. Sections were permeabilized in PBS with 0.25% TritonX-100 (PBST) followed by washes (3 × 10 min) in sodium borohydride in PBS (1 mg/ml) for antigen retrieval. To control for nonspecific binding, sections were washed (3 × 10 min) with PBST and incubated in 10% normal goat serum for 1 hr followed by overnight incubation (4°C) with primary antibody. The next day, sections were washed (3 × 10 min) in PBST and incubated at room temperature (23°C) for 1 hr with either AlexaFlour 594 goat anti-chicken (ThermoFisher Scientific; 1:1,000; RRID:AB_2534099) or AlexFlour 594 goat anti-rabbit (ThermoFischer Scientific; 1:1,000, RRID:AB_2534079), respectively. Afterward, sections were washed (3 × 10 min) in PBST and coverslipped using Fluoromount-G (SouthernBiotech) either with DAPI (α7nAChR) or without DAPI (GFAP/Aβ). To control for staining intensity, all sections were allowed to develop overnight and imaged the following day. Staining intensity was determined using National Institutes of Health Image J Software (v. 1.48; RRID:SCR_003070) to measure a grayscale value within the range of 0–256, where 0 represents white and 256 represents black. Individual templates at two magnifications (10× for GFAP/Aβ; 40× for α7nAChR/DAPI) for the DG, CA3, and CA1 were created and used on all brains similarly. Images were captured with an Olympus 1 × 71 microscope equipped with an Olympus-DP73 video camera system, and a Dell Optiplex 7020 computer. Measurements were performed blinded, and approximately four sections per subregion (DG, CA3, and CA1) were averaged to obtain one value per subject. Amyloid plaques were identified by a dense spherical core of intense staining that were often surrounded by a less compact spherical halo. Staining density was obtained when background staining was subtracted from mean staining intensities on every sixth section through the hippocampus.

2.9 | Data analysis

Sample size was determined based on previous MWM, electrochemical, and immunofluorescence data using C57BL/6J and AβPP/PS1 mice. A power calculation indicated a minimum of 10 mice per group for MWM and electrochemical recordings and five mice per group for immunofluorescent analysis (Hascup et al., 2018) to detect differences with 95% confidence ($a = 0.05$) and 0.8 power. Prism (GraphPad Software, Inc., RRID:SCR_002798) software was used for statistical analyses. To determine if our data plan was appropriate for the collected data, the following assumptions were tested. Significant outliers were identified with a single Grubbs' test (alpha = 0.05) per group. Dependent variables were approximately normally distributed for each group of the independent variable as determined with the Anderson-Darling test as well as visual quantile-quantile plots. A Brown-Forsythe test indicated homogeneity of variances was reasonably met allowing us to proceed with our statistical tests. MWM trial days were analyzed with a two-way ANOVA while the MWM probe challenge, glutamate recordings, and immunofluorescent semiquantification was analyzed with a one-way ANOVA. When the ANOVA indicated a statistically significant main effect, a Dunnett's post hoc analysis was used to determine treatment differences against the AβPP/PS1 vehicle-treated cohort. A two-tailed Student's *t* test was used to compare amyloid plaques in both AβPP/PS1 cohorts. Hippocampal subregions were analyzed independently for glutamate recordings and immunofluorescent semiquantification. Data are represented as mean ± *SEM* and statistical significance was defined as $p < .05$.

3 | RESULTS

3.1 | Riluzole mouse weights

Mice were weighed one week prior to starting treatment and then weekly until treatment completion and again during the MWM. Mice gained weight similarly (Table 1) and weight differences were not observed between treatment groups throughout the study ($F_{2,34} = 0.28$, $p = .75$) supporting that riluzole treatment did not cause nausea-like response.

3.2 | Riluzole cognitive assessment

Six months post riluzole treatment, all mice underwent MWM testing. No differences in swim speed across treatment groups was observed on any training day (Figure 2a) indicating similar motor capabilities. A significant main effect over training days of the corrected integrated path length (CIPL) to the platform (Figure 2b; $F_{4,136} = 17.20$, $p < .0001$) and cumulative distance from the platform (Figure 2c; $F_{4,136} = 16.46$, $p < .0001$) was observed indicating all treatment groups successfully learned the location of the hidden escape platform. Additionally, a main effect of treatment groups was also observed for the CIPL to the platform ($F_{2,34} = 10.99$, $p = .0002$) and cumulative distance from the platform ($F_{2,34} = 10.61$; $p = .0003$). Post hoc analysis indicated that AβPP/PS1 vehicle mice were slower to learn the location of the hidden escape platform compared to both C57BL/6J vehicle and AβPP/PS1 riluzole mice over the first 3 training days. No differences were observed over subsequent training days. Representative tracking plots of the 60-s probe challenge are shown in Figure 2d. During the probe challenge, swim speed was consistent across treatment groups (Figure 2e) indicating differences in memory retention was not a result of motor performance. Analysis of the percentage of time spent in each quadrant indicate a main effect of quadrant occupancy in C57BL/6J vehicle ($F_{3,52} = 15.43$, $p < .0001$), AβPP/PS1 riluzole ($F_{3,40} = 13.42$, $p < .0001$), and AβPP/PS1 vehicle ($F_{3,44} = 17.39$, $p < .0001$). But a post hoc analysis revealed that AβPP/PS1 vehicle mice were the only treatment group to not selectively search the target quadrant for the former location of the hidden escape platform during the probe challenge (Figure 2f). A main effect of the number of annulus 40 entries ($F_{2,34} = 3.36$, $p = .04$) was observed. Post hoc analysis indicated that AβPP/PS1 vehicle mice entered the annulus 40 fewer times compared to C57BL/6J vehicle mice with a trend to improved performance after riluzole treatment (Figure 2g). These data support that 12-month-old AβPP/PS1 vehicle-treated mice have impaired cognition compared to age-matched C57BL/6J mice and that four months of riluzole treatment had long-lasting effects in its ability to rescue learning and memory deficits in AβPP/PS1 mice; similar to normal aging C57BL/6J mice.

3.3 | Riluzole glutamate measures

Representative traces of stimulus-evoked glutamate release are shown in Figure 3a. A main effect on treatment group for basal glutamate (Figure 3b) was observed in the DG ($F_{2,33} = 15.65$, $p < .0001$), CA3 ($F_{2,33} = 9.03$, $p = .0007$), and CA1 ($F_{2,33} = 13.97$, $p < .0001$). A post hoc analysis revealed that AβPP/PS1 vehicle hippocampal basal glutamate was significantly elevated compared to C57BL/6J vehicle and AβPP/PS1 riluzole mice. Similar volumes of 70 mM KCl (Figure 3c) were used to elicit glutamate release in the

TABLE 1 Average percent change of mouse weight during the 4 months of riluzole treatment (3–6 months of age) and at the time of testing (12 months of age)

	Mouse weight percent change (mean ± *SEM*)				
Treatment group	**3 months**	**4 months**	**5 months**	**6 months**	**12 months**
C57BL/6J Vehicle	8.5 ± 0.7	14.0 ± 0.9	18.13 ± 1.5	17.9 ± 2.7	36.2 ± 1.9
AβPP/PS1 Vehicle	7.0 ± 1.1	12.2 ± 2.8	16.3 ± 3.3	16.6 ± 3.4	39.7 ± 3.5
AβPP/PS1 Riluzole	8.2 ± 0.7	13.2 ± 1.0	18.4 ± 1.8	21.7 ± 1.8	39.9 ± 2.6

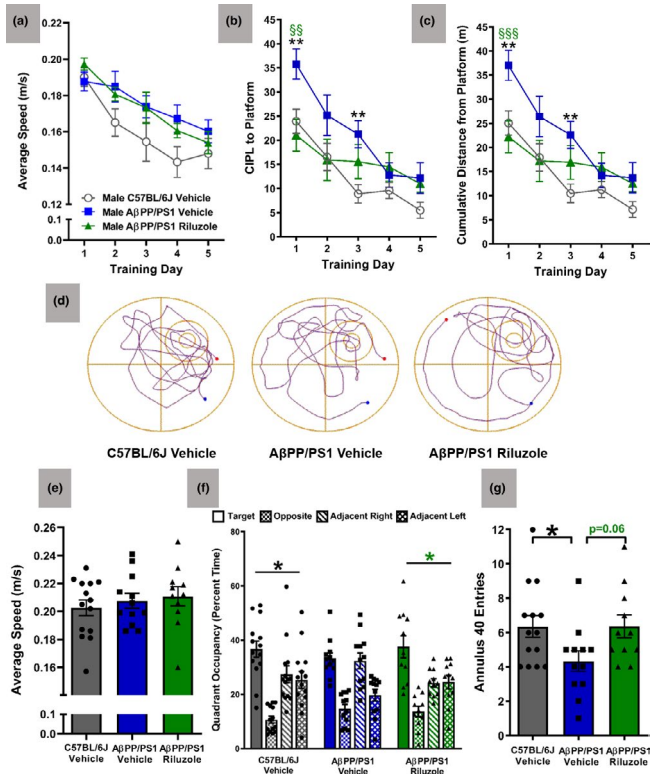

FIGURE 2 MWM training and probe challenge. Mice were trained to locate a hidden escape platform over five consecutive days. Each training day consisted of three trials that were averaged into a single data point for each treatment group to analyze swimming speed (a) CIPL (b) and cumulative distance (c). CIPL adjusts for average swim speed and corrects the difference in distance between different start positions and distance to the platform. Representative track plots of the 60 s probe challenge are shown for each treatment group (d). No differences in swimming speed were observed during the probe challenge (e) indicating motor performance does not account for differences in cognitive measurements. C57BL/6J vehicle and AβPP/PS1 riluzole mice, but not AβPP/PS1 vehicle mice, selectively searched the target quadrant compared to the other quadrants for the former location of the hidden escape platform (f). AβPP/PS1 vehicle mice entered the annulus 40 (immediate area surrounding the platform) fewer times compared to C57BL/6J vehicle and AβPP/PS1 riluzole mice (g). *N* = number of mice. A–c: two-way ANOVA, Dunnett's post hoc; (e–g): one-way ANOVA, Dunnett's post hoc; $^{*}p < .05$, $^{**}p < .01$, AβPP/PS1 vehicle ($n = 12$) versus C57BL/6J vehicle mice ($n = 14$); $^{\S\S}p < .01$, $^{\S\S\S}p < .001$ AβPP/PS1 vehicle versus AβPP/PS1 riluzole mice ($n = 11$)

DG ($F_{2,33} = 0.4905$, $p = .61$), CA3 ($F_{2,33} = 2.43$, $p = .10$), and CA1 ($F_{2,33} = 0.20$, $p = .82$). A main effect of stimulus-evoked glutamate release (Figure 3d) was observed in the DG ($F_{2,33} = 5.77$, $p = .0071$), CA3 ($F_{2,33} = 8.07$, $p = .0014$) and CA1 ($F_{2,33} = 13.87$, $p < .0001$). A post hoc analysis indicated that hippocampal glutamate release was increased in AβPP/PS1 vehicle-treated compared to both C57BL/6J vehicle- and AβPP/PS1 riluzole-treated mice. A main effect on the uptake rate of stimulus-evoked glutamate release (Figure 3e) was observed in the CA3 ($F_{2,33} = 7.16$, $p = .0026$) and CA1 ($F_{2,31} = 5.05$,

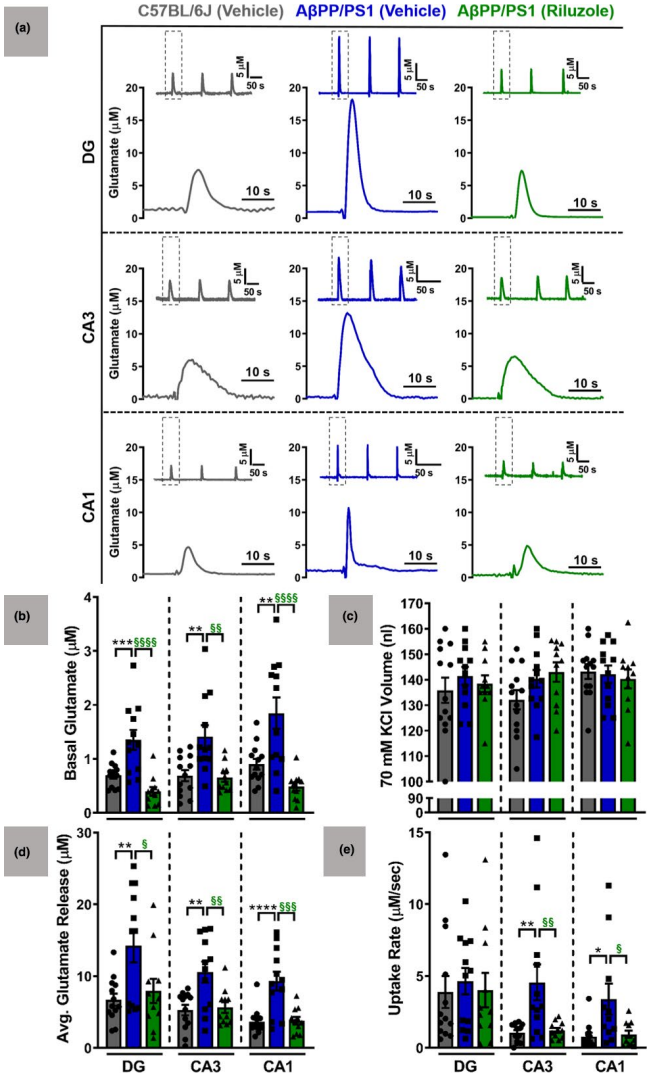

FIGURE 3 Representative glutamate traces and glutamate measures. (a) Representative traces of basal glutamate and stimulus-evoked glutamate release from 70 mM KCl stimulation. Treatment groups are placed into columns and hippocampal subfields are shown in rows. The inset trace at the top of each panel displays the reproducibility of glutamate release and clearance, while the single response is a magnified view of the first inset signal to give a clearer presentation of dynamics of glutamatergic signaling. Concentration and time axes are consistent in all panels for comparisons. (b) Basal glutamate was determined prior to local application of 70 mM KCl in each hippocampal subfield. (c) The volume of stimulus ejected was consistent across treatment groups for direct comparisons of evoked glutamate release. (d) The average glutamate release was determined by subtracting the peak amplitude from the basal measure obtained prior to each ejection of the stimulus. (e) Glutamate uptake rate was calculated by multiplying the peak response (μM) by logarithmic slope (k_{-1}) of glutamate decay versus time (s^{-1}) as estimated by the use of regression analysis ($R^2 \geq 0.9$). *N* = number of mice. A one-way ANOVA with Dunnett's post hoc was used in each hippocampal subfield. $^{*}p < .05$; $^{**}p < .01$, $^{***}p < .001$, $^{****}p < .0001$ AβPP/PS1 vehicle (11–12) versus C57BL/6J vehicle ($n = 12$–13) mice; $^{\S}p < .05$, $^{\S\S}p < .01$, $^{\S\S\S}p < .001$, $^{\S\S\S\S}p < .0001$ AβPP/PS1 vehicle versus AβPP/PS1 riluzole ($n = 11$) mice

$p = .0126$), but not the DG ($F_{2,33} = 0.15$, $p = .86$). A post hoc analysis indicates AβPP/PS1 vehicle mice have a faster glutamate uptake rate compared to both C57BL/6J vehicle and AβPP/PS1 riluzole-treated mice in the CA3 and CA1. These data support that 12-month-old AβPP/PS1 mice have elevated basal glutamate and evoked glutamate release compared to age-matched C57BL/6J mice and that four months of riluzole treatment resulted in attenuated hippocampal glutamatergic tone in AβPP/PS1 mice; similar to levels observed in cognitively normal C57BL/6J mice.

3.4 | Immunofluorescence

3.4.1 | α7nAChR

We previously reported that soluble $A\beta_{42}$ interacts with presynaptic α7nAChRs to stimulate glutamate release in the DG, CA1, and CA3 hippocampal subregions (Hascup & Hascup, 2016). To determine if differences in stimulus-evoked glutamate release were a result of altered α7nAChR density, we used immunofluorescence to measure changes in α7nAChR. The specificity of the α7nAChR primary antibody has been previously demonstrated in α7nAChR knockout mice (Nishio et al., 2017) and a negative control confirming it's specificity in mouse hippocampal tissue is shown in Supplemental Figure 1. Representative images from the CA1 of C57BL/6J vehicle-, AβPP/PS1 vehicle-, and AβPP/PS1 riluzole-treated mice are shown (Figure 4a-I). We observed no significant differences in between treatment groups for each hippocampal subregion (DG: $F_{2,31} = 1.263$, $p = .1992$; CA1: $F_{2,31} = 4.014$, $p = .1068$; CA3: $F_{2,31} = 3.465$, $p = .0811$). Changes in glutamate dynamics across treatment groups was not a result of α7nAChR expression differences, thereby negating potential differences due to $A\beta_{42}$-mediated glutamate release at these receptors.

3.4.2 | GFAP and Aβ plaques staining

Immunofluorescence was used to measure changes in GFAP, while plaque pathology was determined using Amylo-Glo staining reagent. Representative images of C57BL/6J vehicle-, AβPP/PS1 vehicle-, and AβPP/PS1 riluzole-treated mice from the DG (Figure 5a–c; Top) and the CA1/ CA3 (Figure 5d–f; Bottom). Merged images highlight astrogliotic responses surrounding amyloid plaques in both cohorts of AβPP/PS1 mice. GFAP average mean densities for each hippocampal subfield are presented in Figure 5g. No differences in the average mean density of GFAP for each hippocampal subregion were observed, indicating differences in glutamate uptake rate are not attributed to astrocyte density (DG: $F_{2,30} = 1.272$, $p = .2951$; CA1: $F_{2,30} = 0.1813$, $p = .8351$; CA3: $F_{2,30} = 0.4370$, $p = .65$). The number of hippocampal amyloid plaques for both cohorts of AβPP/PS1 mice are shown in Figure 5h. Riluzole treatment had no effect on amyloid accumulation in the DG ($t_{19} = 0.2301$, $p = .82$), CA3 ($t_{19} = 0.4791$, $p = .64$), nor CA1 ($t_{19} = 0.2926$, $p = .77$).

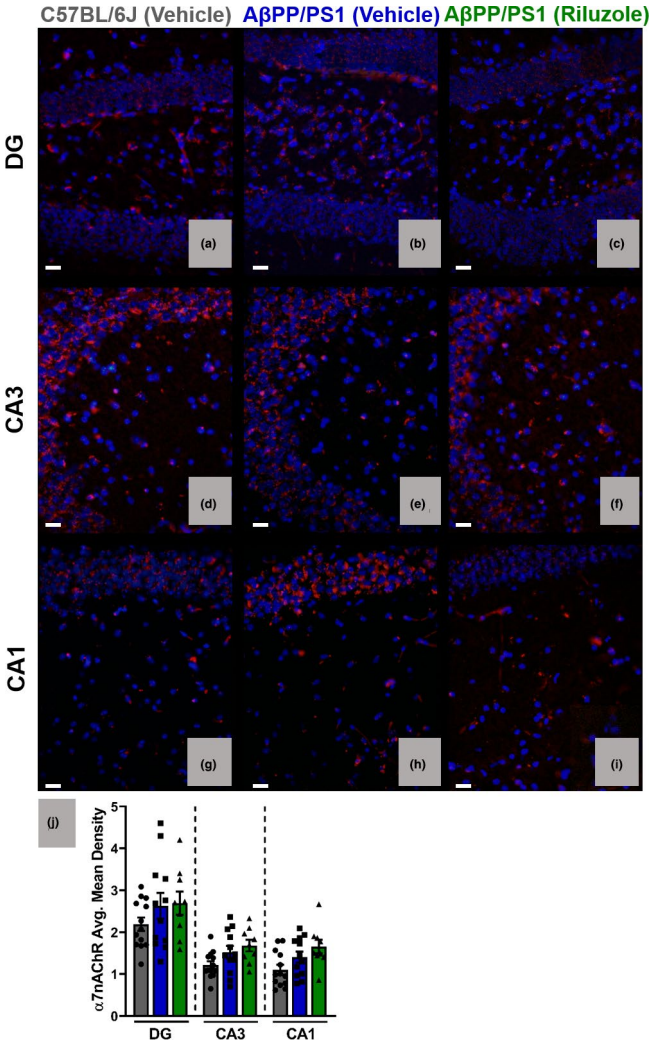

FIGURE 4 Hippocampal α7nAChR expression. (a) Representative 40× images (scale bar = 20 μM) of DAPI (blue) and α7nAChR (red) expression in the DG (a–c), CA3 (d–f), and CA1 (g–i) for the three treatment groups separated into columns. The average mean α7nAChR staining density is shown in (j). A one-way ANOVA with Dunnett's post hoc was used in each hippocampal subfield. *N* = number of mice; C57BL/6J vehicle (*n* = 13), AβPP/PS1 vehicle (*n* = 12); AβPP/PS1 riluzole (*n* = 9) mice

4 | DISCUSSION

Riluzole is a Food and Drug Administration approved drug for the treatment of ALS and is undergoing a Phase II clinical trial for the treatment of mild AD (Clinical Trial #NCT01703117). Riluzole is known to target the glutamatergic system to achieve enhanced glutamate uptake and attenuate glutamate release. Elevated glutamate uptake may be due to improved function/activity of Na^+-K^+-ATPase (Deng et al., 2009), glutamate transporter-1 (Fumagalli et al., 2008), and the glutamate/glutamine (Glu/Gln) cycle (Deng et al., 2009). Immunofluorescent staining for Glt-1 indicated no differences across treatment groups (data not shown). This may indicate riluzole-mediated changes to the Glu/Gln cycle may be several-fold. First,

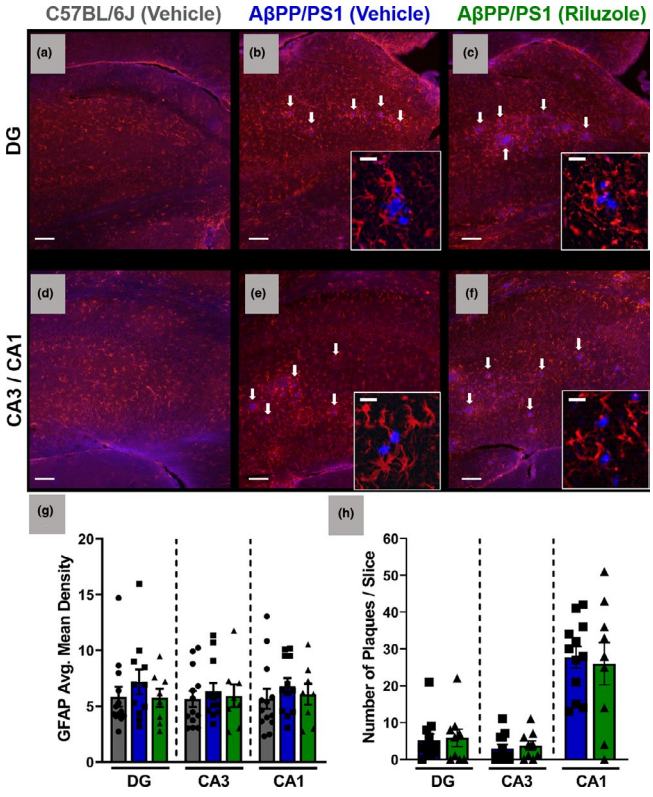

FIGURE 5 Hippocampal GFAP/Aβ expression. (a) Representative 10× images (Scale bar = 100 μM) of GFAP (red) and Aβ plaque (blue) expression, with 40× insets (scale bar = 20 μm), in the DG (a–c) and CA1/CA3 (d–f) hippocampal subregions for the three treatment groups (columns). Subregion-specific changes in GFAP expression (g) was compared using a one-way ANOVA with Dunnett's post hoc, while a *t* test was used for comparing plaque accumulation between riluzole and vehicle treated AβPP/PS1 groups (h). *N* = number of mice

evidence supports enhanced astrocytic glutamine synthetase with riluzole treatment (Deng et al., 2009), which breaks down glutamate to glutamine and may help to stimulate glutamate uptake. Glutamine shuttling from astrocytes to neurons is also increased with riluzole treatment (Chowdhury et al., 2008), however, riluzole also potently inhibits the high-affinity glutamine transport system (Gln/ 2-(methylamino) isobutyrate) responsible for transporting glutamine into neurons (Erickson, 2017), effectively decreasing the glutamine pool in neurons available to produce glutamate. This is further confounded by an increase in glutamate metabolism with more glutamate entering into the tricarboxylic acid cycle (Chowdhury et al., 2008). Together, these actions have a combined effect of increasing glutamate clearance and inhibiting glutamate release, yet it is unclear how long these metabolic actions persist after cessation of drug treatment or if there is a long-term effect on cognition.

We have previously shown that tight regulation of hippocampal glutamatergic signaling is involved in successful aging in a mouse model of longevity and improved healthspan (Hascup et al., 2015, 2016), evoked glutamate release is increased in the CA1 of young (2–4 months old) AβPP/PS1 mice without detectable changes in basal glutamate levels (Hascup et al., 2020), and soluble $A\beta_{42}$, which is one of the earliest detectable biomarkers of AD (Jack et al., 2013), elicits glutamate release (Hascup & Hascup, 2016). More recently, we determined that both evoked glutamate release and basal glutamate levels were elevated throughout the hippocampus by 12 months of age (Hascup et al., 2019). These data support that subregion specific changes to hippocampal glutamate neurotransmission is altered as a function of AD progression. Therefore, targeting the glutamatergic system, specifically by decreasing glutamate release, increasing glutamate clearance, or both, during the prodromal phase may alter disease outcome. Recent studies have shown that riluzole is effective at treating early life stress-induced cognitive decline and synaptic impairments (Lesuis et al., 2019), protects against age-related synaptic alterations related to memory loss (Pereira et al., 2014), and is effective at treating depression in pre-clinical models (Banasr et al., 2010). Furthermore, chronic riluzole treatment reverses gene expression changes observed in microglia, astrocytes, and neurons, and improves memory and pathology in a model of early-onset AD (Okamoto et al., 2018). Previous studies have also shown the restoration of glutamatergic neurotransmission with chronic riluzole treatment in a tau model of AD (Hunsberger et al., 2015). As such, riluzole is an ideal candidate for early therapeutic intervention for AD. However, it is unknown if riluzole has long-term glutamate modulating or procognitive effects. Therefore, we aimed to determine the long-term therapeutic benefits of prodromal riluzole treatment in the AβPP/PS1 mouse model of progressive amyloidosis.

Due to the general lack of success of AD treatments that begin after noticeable onset of cognitive decline our treatment strategy was aimed at early intervention through restoration of glutamatergic signaling prior to cognitive decline. We used riluzole as a prodomal treatment that has the potential alter AD outcome if administered at the earliest signs of altered glutamatergic neurotransmission. The AβPP/PS1 mouse model of AD that we use in the proposal are cognitively normal, lack AD neuropathology, but have elevated glutamate release at 2–4 months of age, begin showing cognitive decline and Aβ plaque accumulation at approximately 6–8 months of age, and have advanced AD neuropathology and are cognitively impaired at 10–12 months. The early four month Riluzole treatment (2–6 months of age) allowed us to complete administration targeting these early changes in glutamatergic neurotransmission prior to measurable cognitive decline in this AD model. The interval between treatment cessation and initiation of cognitive testing allowed us to take advantage of cognitive differences observed at 12 months of age while also examining potential long-term benefits of early intervention aimed at restoring glutamatergic neurotransmission, thereby delaying and/or preventing AD-related cognitive decline.

Consistent with our previous work, glutamatergic dysfunction and decreased cognition were observed in AβPP/PS1 vehicle-treated mice at 12 months of age (Hascup et al., 2018, 2019). Here, we built on that knowledge and show that both basal glutamate and evoked glutamate release are elevated at this time point, supporting alterations to the glutamatergic neurotransmission are in flux as a result of disease progression. Prodromal riluzole treatment from (2–6 months of age), followed by six months without

treatment, rescued basal glutamate and evoked glutamate release in 12-month-old AβPP/PS1 mice to levels consistent with those observed in vehicle-treated normal aging C57BL/6 control mice. AβPP/PS1 riluzole-treated mice also had improved spatial learning and memory performance compared to vehicle-treated genotype-matched mice, indicating that riluzole may have long-term procognitive benefits.

Since we did not observe long-term effects on glutamate neurotransmission or cognition with LY379268 administration under a similar treatment regimen (Hascup et al., 2019), it is unlikely that these effects were mediated through metabotropic glutamate receptor 2/3. Current literature would support a multi-part mechanism to inhibit presynaptic glutamate release and prevent overstimulation of the glutamatergic synapse (Bellingham & Walmsley, 1999; Bellingham, 2011; Ireland et al., 2004; Wang *et al*. 2004). Based on our previous characterizations of glutamatergic neurotransmission during the prodromal period in AβPP/PS1 mice (Hascup et al., 2019; Hascup & Hascup, 2015), inhibition of neuronal excitation during this time should be the most advantageous in preventing subsequent neuronal damage and cognitive decline. However, Hunsberger et al. (2015) demonstrated that riluzole may also be efficacious later in disease progression as it was shown to effectively mediate elevated glutamate neurotransmission in a tau model of AD. Since hyperphosphorylated tau is typically observed later in disease progression, the neuropathological profile for each patient may need to be considered for optimal treatment efficacy.

Previous data support a decrease in GFAP immunoreactivity with riluzole treatment (Carbone et al., 2012b; Fumagalli et al., 2006). In this study, we observed astrocyte clustering around amyloid plaques which has been previously noted (Carbone et al., 2012b; Hascup et al., 2018), but no differences in GFAP mean density in any of the hippocampal subregions with riluzole treatment. The inability of riluzole to reduce GFAP immunoreactivity in this model could possibly be due to the retention of plaque load regardless of treatment. Continuation of plaque accumulation throughout disease progression results in a chronic inflammatory response (Findley et al., 2019; Hascup et al., 2018; Olabarria et al., 2010) that riluzole treatment does not attenuate. Further, we cannot rule out a role of soluble Aβ in chronic inflammation. But, the reported changes in glutamatergic neurotransmission across treatment groups was not a result of α7nAChR expression differences that could have affected soluble $A\beta_{42}$-mediated stimulation.

Overall, the results of this study support the use of riluzole as an early therapeutic intervention strategy to ameliorate cognitive decline and restore glutamatergic tone. Additional studies are ongoing to elucidate riluzole's mechanism of action in this AD model that includes presynaptic and postsynaptic modifications of glutamatergic signaling as well as any sex differences in glutamate-related pathology and response to riluzole treatment.

ACKNOWLEDGMENTS

This work was supported by the National Institutes of Health [NIA R01AG057767 and NIA R01AG061937], the SIU Foundation at the School of Medicine [Harriss and Fannie Belle Roe Malan Research Endowment and the Illinois Health Improvement Association Research Endowment], the Center for Alzheimer's Disease and Related Disorders, the Kenneth Stark Endowment, and the William E. McElroy Foundation.

All experiments were conducted in compliance with the ARRIVE guidelines.

CONFLICT OF INTEREST

The authors declare no conflicts of interest.

AUTHOR CONTRIBUTIONS

KNH conceived the study, conducted the experiments, analyzed the data, and wrote the manuscript. CAF performed plaque analysis, assisted with immunofluorescence imaging, and assisted in writing the manuscript. JB and CAF performed the immunofluorescence and corresponding data analysis and revised the manuscript. SOB performed MWM. KD assisted with statistical interpretation of the data analysis. ST supervised immunofluorescence and revised the manuscript. AB revised the manuscript. ERH conceived and supervised the study and revised the manuscript. All authors approved the final version of the manuscript.

ORCID

Kevin N. Hascup https://orcid.org/0000-0001-6604-1874
Caleigh A. Findley https://orcid.org/0000-0002-8759-1661
Erin R. Hascup https://orcid.org/0000-0003-1037-0809

REFERENCES

Banasr, M., Chowdhury, G. M. I., Terwilliger, R., Newton, S. S., Duman, R. S., Behar, K. L., & Sanacora, G. (2010). Glial pathology in an animal model of depression: Reversal of stress-induced cellular, metabolic and behavioral deficits by the glutamate-modulating drug riluzole. *Molecular Psychiatry*, *15*, 501–511.

Bellingham, M. C. (2011). A review of the neural mechanisms of action and clinical efficiency of riluzole in treating amyotrophic lateral sclerosis: What have we learned in the last decade? *CNS Neuroscience & Therapeutics*, *17*, 4–31.

Bellingham, M. C., & Walmsley, B. (1999). A novel presynaptic inhibitory mechanism underlies paired pulse depression at a fast central synapse. *Neuron*, *23*, 159–170. https://doi.org/10.1016/S0896-6273(00)80762-X

Bromley-Brits, K., Deng, Y., & Song, W. (2011). Morris Water Maze test for learning and memory deficits in Alzheimer's disease model mice. *Journal of Visualized Experiments*, *53*, e2920. https://doi.org/10.3791/2920

Carbone, M., Duty, S., & Rattray, M. (2012a). Riluzole elevates GLT-1 activity and levels in striatal astrocytes. *Neurochemistry International*, *60*, 31–38. https://doi.org/10.1016/j.neuint.2011.10.017

Carbone, M., Duty, S., & Rattray, M. (2012b). Riluzole neuroprotection in a parkinson's disease model involves suppression of reactive astrocytosis but not GLT-1 regulation. *BMC Neuroscience*, *13*, 38. https://doi.org/10.1186/1471-2202-13-38

Chowdhury, G. M. I., Banasr, M., de Graaf, R. A., Rothman, D. L., Behar, K. L., & Sanacora, G. (2008). Chronic riluzole treatment increases glucose metabolism in rat prefrontal cortex and hippocampus. *Journal of Cerebral Blood Flow and Metabolism*, *28*, 1892–1897. https://doi.org/10.1038/jcbfm.2008.78

Deng, Y., Xu, Z., Xu, B., Tian, Y., Xin, X., Deng, X., & Gao, J. (2009). The protective effect of riluzole on manganese caused disruption of glutamate-glutamine cycle in rats. *Brain Research*, *1289*, 106–117. https://doi.org/10.1016/j.brainres.2009.07.012

dos Santos Frizzo, M. E., Dall'Onder, L. P., Dalcin, K. B., & Souza, D. O. (2004). Riluzole enhances glutamate uptake in rat astrocyte cultures. *Cellular and Molecular Neurobiology*, *24*, 123–128.

Erickson, J. D. (2017). Functional identification of activity-regulated, high-affinity glutamine transport in hippocampal neurons inhibited by riluzole. *Journal of Neurochemistry*, *142*, 29–40. https://doi.org/10.1111/jnc.14046

Findley, C. A., Bartke, A., Hascup, K. N., & Hascup, E. R. (2019). Amyloid beta-related alterations to glutamate signaling dynamics during Alzheimer's disease progression. *ASN Neuro*, *11*, 1–20. https://doi.org/10.1177/1759091419855541

Fumagalli, E., Bigini, P., Barbera, S., Paola, M., & De, M. T. (2006). Riluzole, unlike the AMPA antagonist RPR119990, reduces motor impairment and partially prevents motoneuron death in the wobbler mouse, a model of neurodegenerative disease. *Experimental Neurology*, *198*, 114–128. https://doi.org/10.1016/j.expneurol.2005.11.010

Fumagalli, E., Funicello, M., Rauen, T., Gobbi, M., & Mennini, T. (2008). Riluzole enhances the activity of glutamate transporters GLAST, GLT1 and EAAC1. *European Journal of Pharmacology*, *578*, 171–176.

Godyń, J., Jończyk, J., Panek, D., & Barbara, M. (2016). Therapeutic strategies for Alzheimer's disease in clinical trials. *Pharmacology Reports*, *68*, 127–138.

Gourley, S. L., Espitia, J. W., Sanacora, G., & Taylor, J. R. (2011). Antidepressant-like properties of oral riluzole and utility of incentive disengagement models of depression in mice. *Psychopharmacology*, *219*, 805–814. https://doi.org/10.1007/s00213-011-2403-4

Hascup, E. R., Broderick, S. O., Russell, M. K., Fang, Y., Bartke, A., Boger, H. A., & Hascup, K. N. (2018). Diet-induced insulin resistance elevates hippocampal glutamate as well as VGLUT1 and GFAP expression in AβPP/PS1 mice. *Journal of Neurochemistry*. https://doi.org/10.1111/jnc.14634

Hascup, E. R., Wang, F., Kopchick, J. J., & Bartke, A. (2015). Inflammatory and glutamatergic homeostasis are involved in successful aging. *The Journals of Gerontology Series A: Biological Sciences and Medical Sciences*, *71*(3), 281–289.

Hascup, K. N., Britz, J., Findley, C. A., Tischkau, S., & Hascup, E. R. (2019). LY379268 does not have long-term procognitive effects nor attenuate glutamatergic signaling in AβPP/PS1 mice. *Journal of Alzheimer's Disease*, *68*, 1193–1209. https://doi.org/10.3233/JAD-181231

Hascup, K. N., Findley, C. A., Sime, L. N., & Hascup, E. R. (2020). Hippocampal alterations in glutamatergic signaling during amyloid progression in AβPP/PS1 mice. *Scientific Reports*, *10*, 14503.

Hascup, K. N., & Hascup, E. R. (2015). Altered neurotransmission prior to cognitive decline in AβPP/PS1 mice, a model of Alzheimer's disease. *Journal of Alzheimer's Disease*, *44*, 771–776.

Hascup, K. N., & Hascup, E. R. (2016). Soluble amyloid-β42 stimulates glutamate release through activation of the α7 nicotinic acetylcholine receptor. *Journal of Alzheimer's Disease*, *53*, 337–347. https://doi.org/10.3233/JAD-160041

Hascup, K. N., Lynn, M. K., Fitzgerald, P. J., Randall, S., Kopchick, J. J., Boger, H. A., Bartke, A., & Hascup, E. R. (2016). Enhanced cognition and hypoglutamatergic signaling in a growth hormone receptor knockout mouse model of successful aging. *Journals of Gerontology. Series A, Biological Sciences and Medical Sciences*, *72*, 329–337.

Huijbers, W., Mormino, E. C., Schultz, A. P., Wigman, S., Ward, A. M., Larvie, M., Amariglio, R. E., Marshall, G. A., Rentz, D. M., Johnson, K. A., & Sperling, R. A. (2015). Amyloid-β deposition in mild cognitive impairment is associated with increased hippocampal activity, atrophy and clinical progression. *Brain*, *138*, 1023–1035. https://doi.org/10.1093/brain/awv007

Hunsberger, H. C., Weitzner, D. S., Rudy, C. C., Hickman, J. E., Libell, E. M., Speer, R. R., Gerhardt, G. A., & Reed, M. N. (2015). Riluzole rescues glutamate alterations, cognitive deficits, and tau pathology associated with P301L tau expression. *Journal of Neurochemistry*, *135*, 381–394. https://doi.org/10.1111/jnc.13230

Ireland, M. F., Noakes, P. G., & Bellingham, M. C. (2004). P2X7-like receptor subunits enhance excitatory synaptic transmission at central synapses by presynaptic mechanisms. *Neuroscience*, *128*, 269–280. https://doi.org/10.1016/j.neuroscience.2004.06.014

Ishiyama, T., Okada, R., Nishibe, H., Mitsumoto, H., & Nakayama, C. (2004). Riluzole slows the progression of neuromuscular dysfunction in the wobbler mouse motor neuron disease. *Brain Research*, *1019*, 226–236. https://doi.org/10.1016/j.brainres.2004.06.002

Jack, C. R., Knopman, D. S., Jagust, W. J., Petersen, R. C., Weiner, M. W., Aisen, P. S., Shaw, L. M., Vemuri, P., Wiste, H. J., Weigand, S. D., Lesnick, T. G., Pankratz, V. S., Donohue, M. C., & Trojanowski, J. Q. (2013). Tracking pathophysiological processes in Alzheimer's disease: An updated hypothetical model of dynamic biomarkers. *The Lancet Neurology*, *12*, 207–216. https://doi.org/10.1016/S1474-4422(12)70291-0

Lesuis, S. L., Kaplick, P. M., Lucassen, P. J., & Krugers, H. J. (2019). Treatment with the glutamate modulator riluzole prevents early life stress-induced cognitive deficits and impairments in synaptic plasticity in APPswe/PS1dE9 mice. *Neuropharmacology*, *150*, 175–183. https://doi.org/10.1016/j.neuropharm.2019.02.023

Miller, S. L., Fenstermacher, E., Bates, J., Blacker, D., Sperling, R. A., & Dickerson, B. C. (2008). Hippocampal activation in adults with mild cognitive impairment predicts subsequent cognitive decline. *Journal of Neurology, Neurosurgery and Psychiatry*, *79*, 630–635.

Minkeviciene, R., Ihalainen, J., Malm, T., Matilainen, O., Keksa-Goldsteine, V., Goldsteins, G., Iivonen, H., Leguit, N., Glennon, J., Koistinaho, J., Banerjee, P., & Tanila, H. (2008). Age-related decrease in stimulated glutamate release and vesicular glutamate transporters in APP/PS1 transgenic and wild-type mice. *Journal of Neurochemistry*, *105*, 584–594. https://doi.org/10.1111/j.1471-4159.2007.05147.x

Mota, S. I., Ferreira, I. L., & Rego, A. C. (2014). Dysfunctional synapse in Alzheimer's disease – A focus on NMDA receptors. *Neuropharmacology*, *76*, 16–26. https://doi.org/10.1016/j.neuropharm.2013.08.013

Mura, E., Zappettini, S., Preda, S., Biundo, F., Lanni, C., Grilli, M., Cavallero, A., Olivero, G., Salamone, A., Govoni, S., & Marchi, M. (2012). Dual effect of beta-amyloid on α7 and α4β2 nicotinic receptors controlling the release of glutamate, aspartate and GABA in rat hippocampus. *PLoS One*, *7*, e29661. https://doi.org/10.1371/journal.pone.0029661

Nishio, T., Taura, K., Iwaisako, K., Koyama, Y., Tanabe, K., Yamamoto, G., Okuda, Y., Ikeno, Y., Yoshino, K., Kasai, Y., Okuno, M., Seo, S., Sakurai, T., Asagiri, M., Hatano, E., & Uemoto, S. (2017). Hepatic vagus nerve regulates Kupffer cell activation via α7 nicotinic acetylcholine receptor in nonalcoholic steatohepatitis. *Journal of Gastroenterology*, *52*, 965–976. https://doi.org/10.1007/s00535-016-1304-z

O'Brien, J. L., O'Keefe, K. M., LaViolette, P. S., DeLuca, A. N., Blacker, D., Dickerson, B. C., & Sperling, R. A. (2010). Longitudinal fMRI in elderly reveals loss of hippocampal activation with clinical decline. *Neurology*, *74*, 1969–1976. https://doi.org/10.1212/WNL.0b013e3181e3966e

Okamoto, M., Gray, J. D., Larson, C. S., Kazim, S. F., Soya, H., McEwen, B. S., & Pereira, A. C. (2018). Riluzole reduces amyloid beta pathology, improves memory, and restores gene expression changes in a transgenic mouse model of early-onset Alzheimer's disease. *Translational Psychiatry*, *8*, 153.

Okonkwo, O. C., Oh, J. M., Koscik, R., Jonaitis, E., Cleary, C. A., Dowling, N. M., Bendlin, B. B., Larue, A., Hermann, B. P., Barnhart, T. E., Murali, D., Rowley, H. A., Carlsson, C. M., Gallagher, C. L., Asthana, S., Sager, M. A., Christian, B. T., & Johnson, S. C. (2014). Amyloid burden, neuronal function, and cognitive decline in middle-aged adults at risk for Alzheimer's disease. *Journal of the International Neuropsychological Society*, *20*, 422–433.

Olabarria, M., Noristani, H. N., Verkhratsky, A., & Rodríguez, J. J. (2010). Concomitant astroglial atrophy and astrogliosis in a triple transgenic animal model of Alzheimer's disease. *Glia*, *58*, 831–838. https://doi.org/10.1002/glia.20967

Olney, J. W., Wozniak, D. F., & Farber, N. B. (1997). Excitotoxic neurodegeneration in Alzheimer disease. New hypothesis and new therapeutic strategies. *Archives of Neurology*, *54*, 1234–1240.

Parameshwaran, K., Dhanasekaran, M., & Suppiramaniam, V. (2008). Amyloid beta peptides and glutamatergic synaptic dysregulation. *Experimental Neurology*, *210*(1), 7–13.

Parsons, C. G., Stöffler, A., & Danysz, W. (2007). Memantine: A NMDA receptor antagonist that improves memory by restoration of homeostasis in the glutamatergic system–too little activation is bad, too much is even worse. *Neuropharmacology*, *53*, 699–723. https://doi.org/10.1016/j.neuropharm.2007.07.013

Paula-Lima, A. C., Brito-Moreira, J., & Ferreira, S. T. (2013). Deregulation of excitatory neurotransmission underlying synapse failure in Alzheimer's disease. *Journal of Neurochemistry*, *126*, 191–202. https://doi.org/10.1111/jnc.12304

Paxinos, G., & Franklin, K. B. J. (2004). *The mouse brain in stereotaxic coordinates*. Gulf Professional Publishing.

Pereira, A. C., Lambert, H. K., Grossman, Y. S., Dumitriu, D., Waldman, R., Jannetty, S. K., Calakos, K., Janssen, W. G., McEwen, B. S., & Morrison, J. H. (2014). Glutamatergic regulation prevents hippocampal-dependent age-related cognitive decline through dendritic spine clustering. *Proceedings of the National Academy of Sciences of the United States of America*, *111*, 18733–18738.

Ren, S. C., Shao, H., Ji, W. G., Jiang, H. H., Xu, F., Chen, P. Z., Mi, Z., Wen, B., Zhu, G. X., & Zhu, Z. R. (2015). Riluzole prevents soluble Aβ1-42 oligomers-induced perturbation of spontaneous discharge in the hippocampal CA1 region of rats. *Amyloid*, *22*, 36–44.

Talantova, M., Sanz-Blasco, S., Zhang, X., Xia, P., Akhtar, M. W., Okamoto, S., Dziewczapolski, G., Nakamura, T., Cao, G., Pratt, A. E., Kang, Y.-J., Tu, S., Molokanova, E., McKercher, S. R., Hires, S. A., Sason, H., Stouffer, D. G., Buczynski, M. W., Solomon, J. P., … Lipton, S. A. (2013). Aβ induces astrocytic glutamate release, extrasynaptic NMDA receptor activation, and synaptic loss. *Proceedings of the National Academy of Sciences of the United States of America*, *110*, E2518–E2527.

Wang, S. J., Wang, K. Y., & Wang, W. C. (2004). Mechanisms underlying the riluzole inhibition of glutamate release from rat cerebral cortex nerve terminals (synaptosomes). *Neuroscience*, *125*, 191–201. https://doi.org/10.1016/j.neuroscience.2004.01.019

Webster, S. J., Bachstetter, A. D., Nelson, P. T., Schmitt, F. A., Eldik, L. J., & Van Eldik, L. J. (2014). Using mice to model Alzheimer's dementia: An overview of the clinical disease and the preclinical behavioral changes in 10 mouse models. *Frontiers in Genetics*, *5*, 1–14. https://doi.org/10.3389/fgene.2014.00088

Winblad, B., & Poritis, N. (1999). Memantine in severe dementia: Results of the9M-best study (benefit and efficacy in severly demented patients during treatment with memantine). *International Journal of Geriatric Psychiatry*, *14*, 135–146.

Yang, T., Li, S., Xu, H., Walsh, D. M., & Selkoe, D. J. (2017). Large soluble oligomers of amyloid β-protein from Alzheimer brain are far less neuroactive than the smaller oligomers to which they dissociate. *Journal of Neuroscience*, *37*, 152–163. https://doi.org/10.1523/JNEUROSCI.1698-16.2016

Yang, Y., Ji, W., Zhang, Y., Zhou, L., Chen, H., Yang, N., & Zhu, Z. (2020). Riluzole ameliorates soluble Aβ1–42-induced impairments in spatial memory by modulating the glutamatergic/GABAergic balance in the dentate gyrus. *Progress in Neuro-Psychopharmacology and Biological Psychiatry*, 110077. [Epub ahead of print]. https://doi.org/10.1016/j.pnpbp.2020.110077

SUPPORTING INFORMATION

Additional supporting information may be found online in the Supporting Information section.

How to cite this article: Hascup KN, Findley CA, Britz J, et al. Riluzole attenuates glutamatergic tone and cognitive decline in AβPP/PS1 mice. *J Neurochem*. 2020;00:1–11. https://doi.org/10.1111/jnc.15224